Sensors & Actuators: B. Chemical 331 (2021) 129414

Contents lists available at ScienceDirect

Sensors and Actuators: B. Chemical

journal homepage: www.elsevier.com/locate/snb

Virtual sensor array based on MXene for selective detections of VOCs

Dongsheng Li [a], Guang Liu [b], Qian Zhang [a], Mengjiao Qu [a], Yong Qing Fu [c], Qingjun Liu [b], Jin Xie [a,*]

[a] State Key Laboratory of Fluid Power and Mechatronic Systems, Zhejiang University, Hangzhou, Zhejiang, 310027, China
[b] Biosensor National Special Laboratory, Key Laboratory for Biomedical Engineering of Education Ministry, Department of Biomedical Engineering, Zhejiang University, Hangzhou, 310027, PR China
[c] Faculty of Engineering and Environment, University of Northumbria, Newcastle upon Tyne, NE1 8ST, UK

ARTICLE INFO

Keywords:
MXene
2D material
Cross-sensitivity
Virtual sensor array
Multivariable VOC sensing
Broadband impedance spectra

ABSTRACT

Two-dimensional transition metal carbides/nitrides, known as MXenes, have recently received significant attention for gas sensing applications. However, MXenes have strong adsorption to many types of volatile organic compounds (VOCs), and therefore gas sensors based on MXenes generally have low selectivity and poor performance in mixtures of VOCs due to cross-sensitivity issues. Herein, we developed a $Ti_3C_2T_x$-based virtual sensor array (VSA) which allows both highly accurate detection and identification of different VOCs, as well as concentration prediction of the target VOC in variable backgrounds. The VSA's responses from the broadband impedance spectra create a unique fingerprint of each VOC without a need for changing temperatures. Based on the methodologies of principal component analysis and linear discrimination analysis, we demonstrate highly accurate identifications for different types of VOCs and mixtures using this MXene based VSA. Furthermore, we demonstrate an accuracy of 93.2% for the prediction of ethanol concentrations in the presence of different concentrations of water and methanol. The high level of identification and concentration prediction shows a great potential of MXene based VSA for detection of VOCs of interest in the presence of known and unknown interferences.

1. Introduction

Gas sensing has attracted considerable research interests in recent years [1–3], and sensitive and selective gas detection becomes critical in agriculture, pollution monitoring, food quality assurance, and medical diagnosis [4–6]. In particular, detection of volatile organic compounds (VOCs) in exhaled breath of human is regarded as a promising method for early diagnosis of illness [7]. Around 200 VOCs have been detected in human breath and their contents reflect the person's physical conditions [8]. Accordingly, gas sensors are required not only to sensitively detect an individual VOC but also to effectively distinguish different VOCs and quantify the specific target VOC in the presence of a complex background.

Typically, a sensing material is deposited on the gas sensor and the properties of this sensing layer greatly affect the responses of gas sensors. Two-dimensional (2D) materials [9], such as graphene [10,11], MoS_2 [12,13], and black phosphorus (BP) [14] are among the most promising materials for gas sensing applications, because of their large surface area, versatile surface chemistry, and capability of sensitive detection at room temperature. Recently, gas sensors based on a new family of 2D materials called MXene have also shown promising performance [15,16].

MXenes, with a molecular formula of $M_{n+1}X_nT_z$, are generally synthesized by etching the intermediate layer (A) of a $M_{n+1}AX_n$ phase [17–19], in which M, A, X, and T represent transition metal (e.g., titanium, vanadium), intermediate element (e.g., aluminum, silicon), C or N element, and surface group (e.g., OH-, F-), respectively. As one of the 2D transition metal carbides/nitrides, MXenes possess a metallic conductivity, while their surfaces are covered with functional groups. Such a good combination makes MXene based gas sensors having ultrahigh signal-to-noise ratios and low limit of detection (LOD) compared with those based on the other 2D materials [20]. Interestingly, it was also reported that $Ti_3C_2T_x$ based gas sensors show a better response to VOCs over the oxidizing gases [21].

However, MXenes have strong adsorptions to many types of VOCs. Currently most MXene based sensors are based on measurements of

* Corresponding author.
E-mail address: xiejin@zju.edu.cn (J. Xie).

https://doi.org/10.1016/j.snb.2020.129414
Received 12 November 2020; Received in revised form 23 December 2020; Accepted 24 December 2020
Available online 4 January 2021
0925-4005/© 2021 Elsevier B.V. All rights reserved.

changes in their electrical resistances (or often called chemiresistors), but they are ineffective for sensing of VOC mixtures due to issue of cross-sensitivity [22–24]. The selectivity of these MXene based sensors remains a key challenge. The poor selectivity of individual conventional sensor can be mitigated through combining sensors into arrays, which is sometimes referred as an "electronic nose" [25,26]. However, increasing number of sensors in the sensor array increases the power consumption and complicates the device's circuitry and computation [27]. Additionally, the higher the number of sensing elements, the higher the chances of breakdown for the sensor array [28].

To overcome these drawbacks, a recent breakthrough comes from the virtual sensor array (VSA), in which one individual sensor can be used to generate multi-dimensional signals similar to those produced by the electronic nose [29]. These multi-dimensional signals could produce unique responsive patterns for different VOCs [30]. To facilitate accurate identification of each VOC, pattern recognition techniques, such as principal component analysis (PCA) [27], linear discriminant analysis (LDA) [31], and partial least squares (PLS) [29] are often applied. These reported VSAs are mostly relied on varying the temperature of the sensing element to overcome cross-sensitivity of those sensors based on the measurement of resistance (or capacitance) [32–34]. Nevertheless, the time to reach the targeted temperature is often too long for many real applications. Besides, a permanent change of material properties for the sensing layer may occur when temperature cycling is applied.

Currently most gas sensors only detect changes of a single property (e.g., resistance or capacitance) of the sensor, whereas changes of other electrical properties from the sensors are often ignored, thus resulting in a significant loss of valuable information. The impedance spectra measurement is possible to provide electric properties of a bulk and an interface which we cannot easily obtain from direct current (DC) signals [35]. On one hand, impedance spectra have usually been used to analyze the electrical process of gas sensors and understand the gas sensing mechanism [36]. On the other hand, they are rarely used for quantitative sensing, just like resistance or capacitance measurements. The impedance spectra of VOC sensors can be used to distinguish different types of VOCs. For example, Liu et al. have detected impedance changes using a gas sensor at different frequencies of 19.9 kHz and 2.1 kHz, respectively, and managed to distinguish between formaldehyde and acetone [37].

Herein, we propose a $Ti_3C_2T_x$ based VSA which allows highly accurate detection and identification of different types of VOCs, as well as estimation of concentration for a single VOC within a multiple VOCs mixture. In this method, we deposited a thin film of $Ti_3C_2T_x$ on the surface of an interdigital electrode (IDE) to form a VSA, which was then exposed to a range of different VOCs with various concentrations at room temperature. The broadband impedance spectra of the $Ti_3C_2T_x$ based VSA were obtained at various conditions. They were then used as the inputs for supervised and unsupervised machine learning, and the impedance responses from the VSA obtained at different frequencies were analyzed systematically using PCA, LDA, and PLS regression. The high accuracy of identification and concentration estimation shows the potential of MXene based VSAs for detection of VOCs in the presence of a variable background. To the best of our knowledge, this is the first report of a VSA based on MXene and broadband impedance spectra.

2. Experimental section

2.1. Fabrication of MXene based VSA

A schematic illustration of the fabricated $Ti_3C_2T_x$ based sensor is shown in Fig. 1a. The sensor was prepared by covering the fabricated IDE with a layer of $Ti_3C_2T_x$. Two atomic layers of carbon were sandwiched between three atomic layers of titanium in the $Ti_3C_2T_x$ structure. With a typical synthesis method, we expect that the surface of $Ti_3C_2T_x$ would be randomly terminated with hydroxyl (—OH), oxygen (—O), and fluorine (—F) groups [15]. Detailed synthesis processes of $Ti_3C_2T_x$ have been presented in S1 of Supplementary Material. An IDE was made on Al_2O_3 ceramic substrate (5 mm × 5 mm) with 11 pairs of interdigitated Au/Ni/Cu electrodes (thicknesses of 10 μm/4 μm/ 1 μm). The distances among Au strips and their widths were both 100 μm. A dispersion (20 μL) of $Ti_3C_2T_x$ in deionized water with a concertation of 0.05 mg/mL was dropped on the prepared IDEs and dried in a vacuum chamber, thus forming a sensing layer.

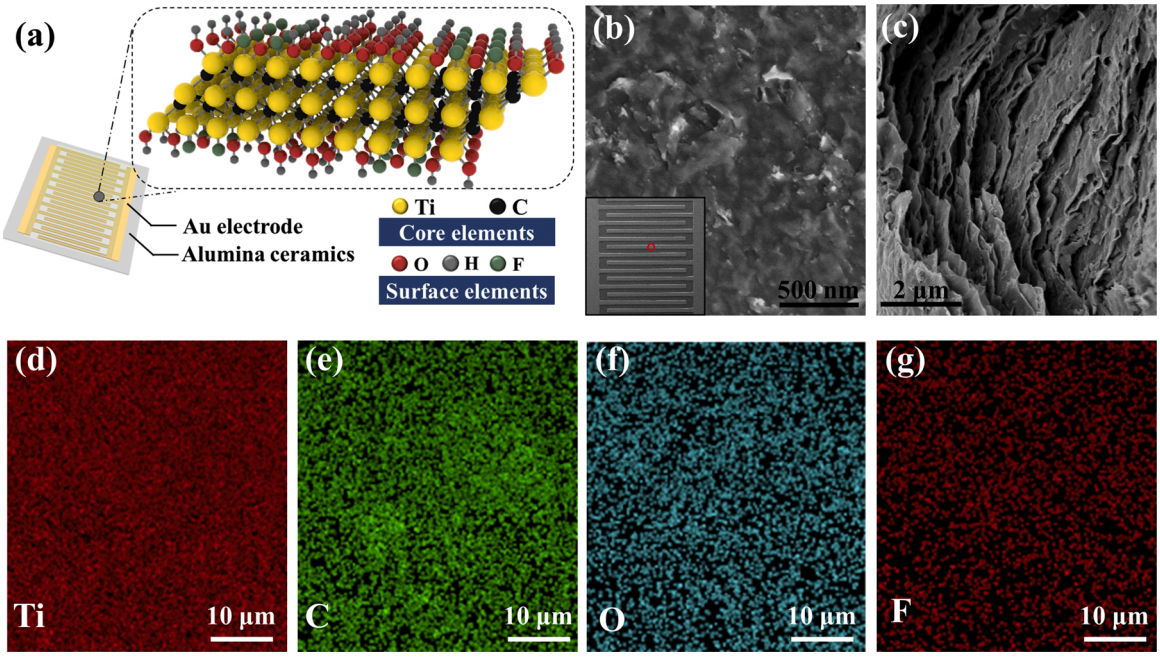

Fig. 1. Schematic illustration and morphological characterization of the $Ti_3C_2T_x$ film. (a) Schematic illustration of the $Ti_3C_2T_x$ film based sensor. (b) SEM image of the $Ti_3C_2T_x$ based sensor surface. (c) Cross-section view of the $Ti_3C_2T_x$ film. (d-g) Elemental mapping analyses of $Ti_3C_2T_x$ film: (d) Ti, (e) C, (f) O, (g) F.

2.2. Material characterizations

A field emission scanning electron microscope (FE-SEM; SU-8100, Hitachi) equipped with an energy dispersive X-Ray spectrometer (EDS; X-max80, Oxford) was used to study the surface morphology of the produced sensing film and distribution of elements. The thickness of the MXene film was measured using a profilometer (KLA/Tencor D-100). An X-ray diffractometer (MAXima XRD-7000, Shimadzu) was used for X-ray diffraction (XRD) analysis. X-ray photoelectron spectroscopy (XPS, Escalab 250Xi, Thermo Fisher) was used to characterize the chemical components and chemical bonding structures of the $Ti_3C_2T_x$ film. XPS analysis was conducted through curve fitting and calculations using Gaussian–Lorentzian method.

2.3. Gas sensing system

A schematic illustration of VOC sensing experimental setup is shown in Fig. S1. The sensing experiment was performed at room temperature (25℃). The sensing performance was investigated by exposing the $Ti_3C_2T_x$ based VSA to various concentrations of the targeted VOCs. The desired VOC concentration was obtained by injecting the required quantity of anhydrous liquid analytes into a sealed glass container using a microliter syringe. The concentrations of targeted VOCs in the chamber were calculated using the following equation [38,39]:

$$C = \frac{22.4\rho TV_s}{273MV} \times 1000 \quad (1)$$

where C is the concentration of the gaseous VOC at the room temperature (ppm), ρ is the density of anhydrous liquid VOC (g· mL^{-1}), T is the testing temperature (K), Vs is the volume of anhydrous liquid VOC (μL), M is the molecular weight of a VOC (g· mol^{-1}), and V is the volume of the glass container (L) filled with the VOC. In this work, taking ethanol as an example, the values of M, ρ and T are 46 g· mol^{-1}, 0.789 g· mL^{-1} and 298 K, respectively. Dry air was supplied from an air cylinder and the container was cleaned by dry air flow at room temperature before doing each gas sensing test. The broadband impedance spectra (with frequencies from 20 Hz to 2 MHz) were measured using an LCR meter (Keysight E4980A). The response was defined as the relative change in the impedance of the VSA after exposure to VOCs compared to the baseline impedance (ΔR (X) /R_0 (X_0) (%)). Response and recovery time can be defined as the time from when the impedance starts to change until the impedance reaches 90% of its final value. The LOD value, i.e. the lowest concentration of target gas that can be distinguished from the common atmosphere, was calculated based on the signal-to-noise ratio (S/N > 3).

2.4. Analysis of $Ti_3C_2T_x$ based VSA data

Predictive models were developed using eight representative parameters obtained from the broadband impedance spectra, i.e. using the resistance values at 20 Hz, 336 kHz, 2 MHz and the reactance values at 189 kHz, 299 kHz, 710 kHz, 1.19 MHz, 2 MHz. First, PCA was applied for classification of multivariate data and reducing the dimensionality of the original data set. PCA is a powerful unsupervised analysis tool that basically projects the data points into a new coordinate system, whose coordinates account for the largest variance in the original data [27]. It allows a qualitative survey of the discriminating power of the VSA. The LDA was performed as a supervised pattern recognition tool meaning that the correct classification is known for each object [31]. The resultant principal components in the PCA were used as input variables to the LDA to quantitatively identify different test analytes. A cross-validation method was used to estimate the identification. To quantify concentrations of individual vapor in a mixture, we applied PLS with five latent variables (LVs). The PLS determines correlations between the independent variables (ethanol concentration) and the VSA's response by finding the direction that explains the maximum variance of the independent variables in the multidimensional space of the sensor response [29]. Multivariate data processing (PCA, LDA and PLS) was carried out using MATLAB programs in this study.

3. Results and discussion

3.1. Material characterizations

Surface morphology of the $Ti_3C_2T_x$ based sensor is shown in Fig. 1b and optical microscope images of the obtained sensor are shown in Figs. S2a and S2b, which reveal a uniform layer of the deposited $Ti_3C_2T_x$. The thickness of the MXene films on the surface of three devices is about 240 nm, as shown in Fig. S2c, indicating a good repeatability. A cross-sectional SEM image of the $Ti_3C_2T_x$ film is shown in Fig. 1c, which is produced through vacuum filtration of the same $Ti_3C_2T_x$ solution used for the sensor fabrication. The observed layered structure is due to the ordered stacking of individual layers of $Ti_3C_2T_x$, which results in increased surface-to-volume ratio, potentially contributing to a large sensing response. Fig. 1d to g show the EDS analysis of the deposited $Ti_3C_2T_x$ film. The core elements (Ti, C) and surface elements (O, F) are evenly distributed across the entire film. These results indicate a uniform deposition of $Ti_3C_2T_x$ on the device surface.

XRD measurements of the $Ti_3C_2T_x$ film reveal a sharp peak at $2\theta = 6.7^\circ$ as shown in Fig. 2a. There are no peaks related to Ti_3AlC_2 in MAX phase, indicating that $Ti_3C_2T_x$ was successfully transformed from Ti_3AlC_2. This sharp peak corresponds to the (002) peak of $Ti_3C_2T_x$ with a center-to-center distance of 13.3 Å. Given the thickness of one atomic layer (~10 Å), the free interlayer spacing is roughly 3.3 Å, which is in a good agreement with the previously reported results [40].

Fig. 2b to d show a set of high-resolution XPS spectra (Ti 2p, C 1s, O 1s) of $Ti_3C_2T_x$. The Ti 2p spectrum (Fig. 2b) can be fitted with four doublets (Ti 2p1/2, Ti 2p3/2) with an area ratio of 1:2, and the doublet separation is 5.8 eV. The binding energies of Ti—C (Ti^+), Ti—X (Ti^{2+}), Ti_xO_y (Ti^{3+}), and TiO_2 (Ti^{4+}), are 454.88, 455.85, 457.42, and 459.05 eV, respectively. The Ti—X corresponds to sub-stoichiometric titanium carbides or titanium oxy-carbides, which is in a good agreement with previous XPS studies [20]. The C 1s spectrum shown in Fig. 2c can be deconvoluted into four peaks centered at 281.66, 284.8, 285.41, and 288.7 eV, corresponding to C—Ti, C—C, CHx/CO and —COO, respectively [41]. The O 1s spectrum in Fig. 2d can be deconvoluted into four peaks centered at 529.77, 531.57, 533.6, and 533.92 eV, corresponding to TiO_2, sub-stoichiometric TiO_x, Ti—OH, and adsorbed H_2O on the surface, respectively [20]. These results confirm that the surface of the $Ti_3C_2T_x$ nanosheet is indeed terminated by many types of functional groups (—OH, —O, —F, etc.), facilitating its adsorption of VOCs.

3.2. Dynamic VOC sensing

The resistance responses of the sensor operated at 20 Hz with the continuous changes of ethanol concentrations were firstly investigated. The resistance values were continuously recorded with a time interval of 1 s and the data showed a good tracking performance of the sensor as the ethanol concentration was continuously changed, as indicated in Fig. 3a. The short-term repeatability performance of the $Ti_3C_2T_x$ based sensor operated at 20 Hz was further studied by repeatedly changing the ethanol concentration between 0 and 100 ppm, and the results are shown in Fig. 3b. The short-term repeatability performance of the sensor operated at other frequencies are shown in Fig. S3. A good repeatability was obtained over several cyclic tests at all frequencies. The response and recovery speeds of the sensor were investigated by rapidly changing the ethanol concentration between 0 and 100 ppm, and detailed response and recovery processes of the sensor are shown in Fig. 3c and d. According to the definitions mentioned previously, the response and recovery times of the sensor are 59 s and 71 s, respectively. The resistance values of the sensor operated at 20 Hz were further recorded when

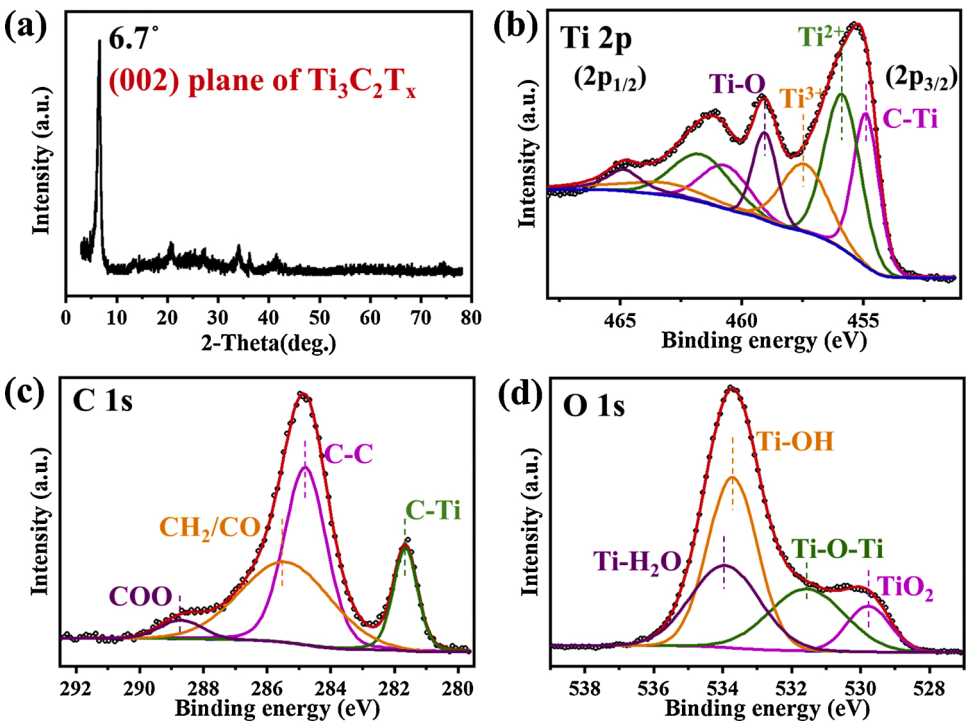

Fig. 2. Structural and chemical characterizations of $Ti_3C_2T_x$. (a) XRD patterns of $Ti_3C_2T_x$. (b-d) XPS of $Ti_3C_2T_x$ at three core levels: (b) Ti 2p, (c) C 1s, (d) O 1s.

the ethanol concentration was fixed at different levels (i.e., 100 ppm and 200 ppm), as shown in Fig. 3e. There is only a very small fluctuation in the resistance values. Fig. S4 shows fluctuations in the impedance of sensor operated at different frequencies when the concentration of ethanol is zero. Theoretical LOD values of the sensor to ethanol are 862 ppb, 780 ppb, 791 ppb, respectively, obtained based on the values of resistance at 20 Hz, reactance at 299 kHz, and reactance at 2 MHz, respectively.

Fig. 3f displays the responses of $Ti_3C_2T_x$ based sensor exposed to different VOCs, i.e., 100 ppm of methanol (MeOH), ethanol (EtOH), acetone, isopropanol (IPA), acetonitrile (MeCN), dichloromethane (DCM), hexane, and toluene (TOL). Prior to exposure to the target VOCs, the sensor was exposed to dry air for at least 10 min, in order to stabilize the baseline impedance. Then the sensor was exposed to the target VOCs for 150 s. The $Ti_3C_2T_x$ based sensor display all positive changes of the resistance, indicating that the channel of charge carrier transport was hindered when VOC molecules were adsorbed.

3.3. VOCs fingerprints and working principle of VSA

The $Ti_3C_2T_x$ based VSA was exposed to eight different VOCs as mentioned above with different concentrations from 100 ppm to 800 ppm, and the broadband impedance spectra were measured. Based on the impedance spectra obtained, we selected eight representative parameters mentioned above as the VOC characteristics.

A data set of impedance responses can be directly used as a VOC's unique fingerprint by collecting changes of the eight parameters in different VOC concentrations, which is shown in Fig. S5. Resistance values at 20 Hz, 336 kHz, 2 MHz and reactance values at 189 kHz, 299 kHz exhibit positive responses, whereas the reactance values at 710 kHz, 1.19 MHz, 2 MHz exhibit negative responses on exposure to different VOCs. In addition, the response amplitudes of all the sensing parameters increase as the concentrations of VOCs are increased. The increasing slope is much higher at a low concentration of the VOCs. Apparently, different VOCs lead to different response patterns as shown in Fig. S5, which provides the critical information for a simple and straightforward identification of a specific type of VOC.

In order to visualize the unique response patterns of different VOCs, the changes of different characteristic parameters versus different VOC concentrations are depicted in a contour plot, as shown in Fig. 4. It clearly shows that a discernable discrepancy exists between the patterns of different VOCs. Therefore, we can confirm that the multi-parameters sensing responses create a unique fingerprint for each VOC, which can then be used for identification of the type of VOC.

The experimental Nyquist curve over a frequency range of 20 Hz-2 MHz of the proposed VSA in dry air is shown in Fig. S6a. The shape of the curve clearly indicates that the circuit model of the sensor is composed of several parts [42]. The equivalent circuit model of the $Ti_3C_2T_x$ based VSA is shown in Fig. S6b. Here the circuit element *R1* represents the contact resistance; the circuit elements *R2* and *L* represent the resistance in thickness direction and inductance between $Ti_3C_2T_x$ layers; and elements *R3* and *C* represent the transverse resistance and capacitance between electrodes. Fig. S6a shows that the fitting data are very close to the experimental data, indicating the equivalent circuit model is accurate. In the circuit model, the AC resistance (*R(f)*) and reactance (*X(f)*) can be written as:

$$R(f) = R1 + \frac{(2\pi f)^2 L^2 R2}{R2^2 + (2\pi f)^2 L^2} + \frac{R3}{1 + (2\pi f)^2 C^2 R3^2} \quad (2)$$

$$X(f) = \frac{2\pi f L R2^2}{R2^2 + (2\pi f)^2 L^2} - \frac{2\pi f C R3^2}{1 + (2\pi f)^2 C^2 R3^2} \quad (3)$$

The sensing mechanism of a $Ti_3C_2T_x$-based sensor is related to the absorption of the VOCs by both defects and functional groups. Some VOCs are bonded on the structural defects of the $Ti_3C_2T_x$ nanosheets, and some are bonded and interacted with surface functional groups such as —O and —OH [8]. On the other hand, intercalation of molecules from gas phase into MXene interlayers can increase the layer spacing of MXene, and will play a crucial role in determining the response of VOC sensing [21]. Various effects lead to the change of properties of the sensor which correspond to different components in the equivalent circuit model. The proportions of various effects caused by different VOCs are quite different, and each VOC has an effect of specific proportion on multiple components in the equivalent circuit model [5,43].

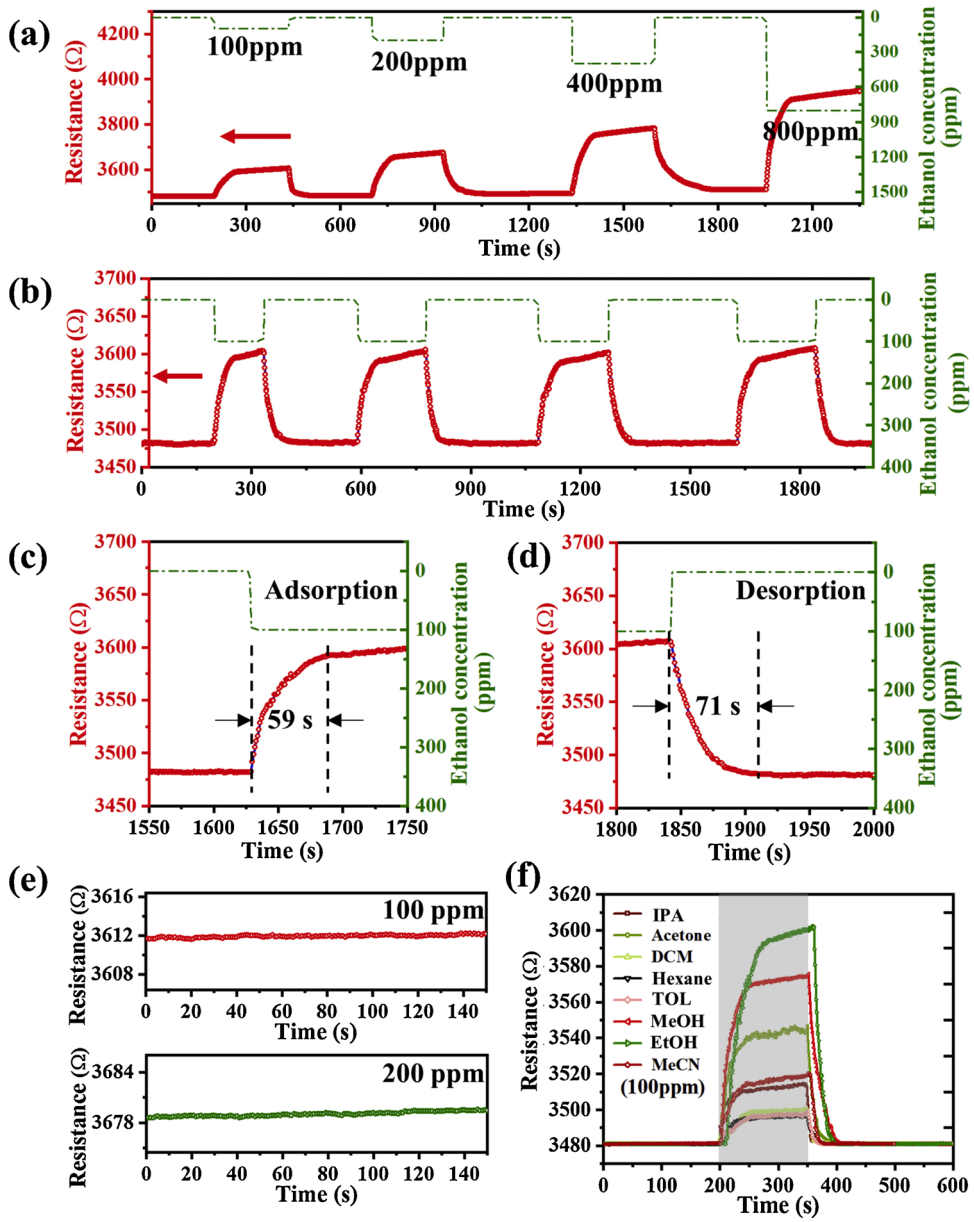

Fig. 3. Dynamic response test of the $Ti_3C_2T_x$ film based VOC sensor. (a) Continuous response of the resistance of sensor to different ethanol concentrations. (b) Short-term repeatability of sensor when the ethanol concentration is repeatedly changed. Detailed response (c) and recovery (d) processes of the sensor. (e) Fluctuations in the resistance of sensor at fixed ethanol concentration levels. (f) Resistance variation upon exposure to 100 ppm of 8 VOCs.

The impedance value obtained at each frequency is determined by all the components in the equivalent circuit model and the influences of changes of every component on impedances (*R(f)* and *X(f)*) are affected by frequency, which is shown clearly in Eqs. (2) and (3). As long as the influences of two VOCs on each component are not the same, the changes of impedance spectra will be different. Based on these different changes, VOC fingerprints can be generated using the multi-parameters sensing responses based on the results of broadband impedance spectra. Fig. S7 shows a block diagram of the sensing mechanism of the VSA. Several hypothetical examples are shown in Table S1.

3.4. Dimensionality reduction of raw data and unsupervised classification of VOCs

We performed the PCA to discriminate the VOCs with the similar responses and determine the dimensions of the resulting data set of multi-parameters sensing responses. The responses of the two groups VOCs (i.e., the oxygenated and non-oxygenated VOCs) were analyzed by PCA separately. By performing the PCA on these multi-parameters data, high contributions of the first three principle components (PCs) were achieved: i.e., 76.6%, 15.7% and 7.6% (oxygenated VOCs); 87.7%, 8.9% and 3.2% (non-oxygenated VOCs), for PC1, PC2, PC3, respectively. This shows that the high data dimensionality can be obtained from the VSA on exposure to only four vapors.

Fig. 5 shows a 3D plot of the first 3 PCs keeping most of the information (accounting for a total of 99.8%). Each point corresponds to an entire fingerprint of a VOC at a specific concentration (consists of eight parameters) and is colored according to the VOC it represents. We project two types of overlapping VOCs in this view on the coordinate plane. Points belonged to different VOCs are well-separated in space, as can be seen in Fig. 5, indicating that the sensor can differentiate the VOCs very well. Points belonged to same VOC but with the different concentrations (from 100 ppm to 800 ppm) are located approximately in one line. These results show that the VSA has a high data dimensionality

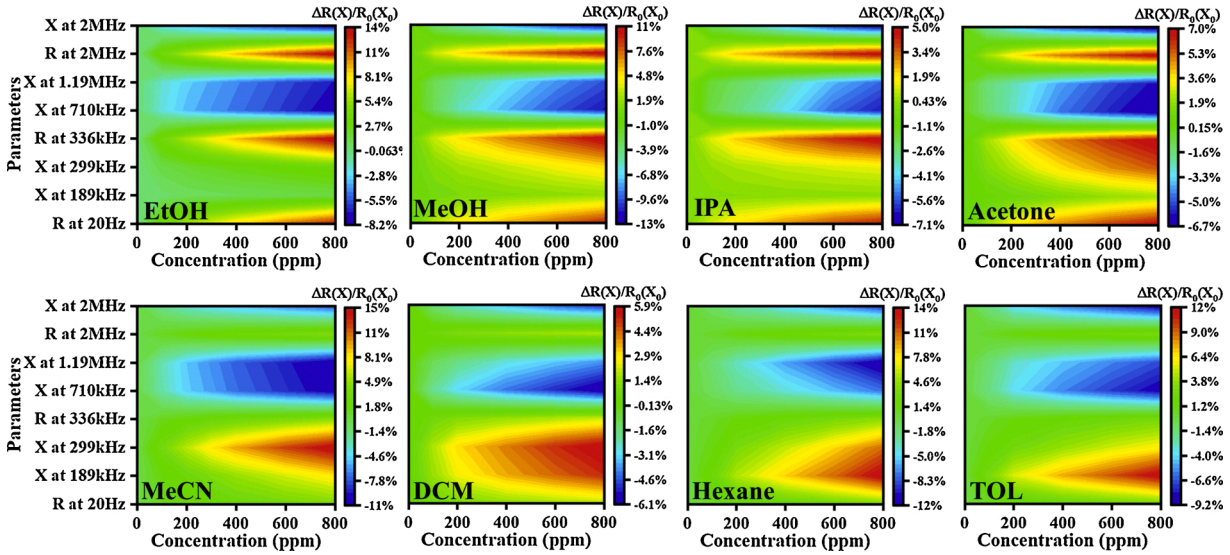

Fig. 4. Contour plot of unique fingerprint patterns of different VOCs.

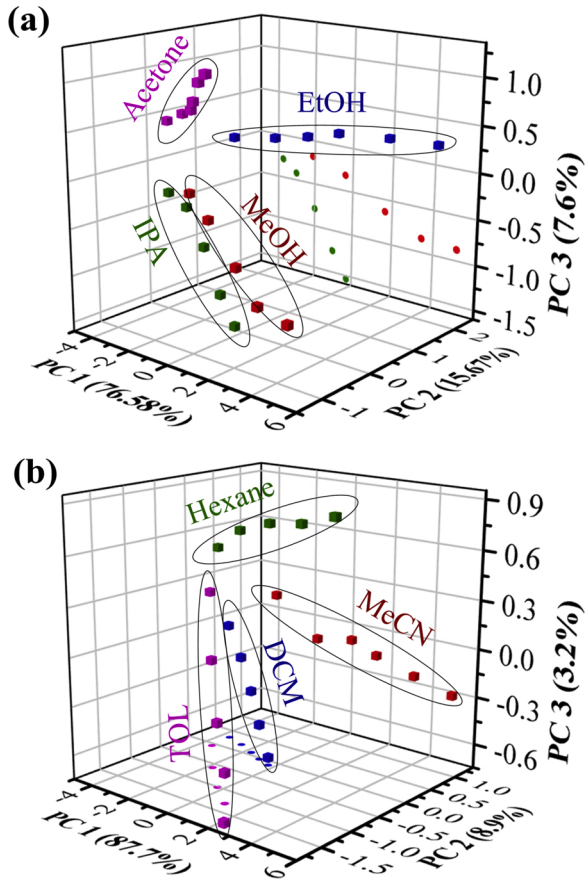

Fig. 5. 3D plot of the first 3 principal components of oxygenated (a) and non-oxygenated (b) VOCs.

and a potential to distinguish between different VOCs and quantify concentrations of individual vapors.

3.5. Supervised gas identification

To quantitatively identify the types of various VOCs, LDA was carried out for oxygenated and non-oxygenated VOCs, respectively. Fig. 6a shows a 3D plot of LDA results of the oxygenated VOCs. Each point is colored according to the VOC type and a pentagram represents the center of mass of each points group. Results shown in Fig. 6a clearly indicate that each VOC can be well determined. The LDA results of oxygenated VOCs are depicted in Fig. 6b. LDA identification accuracies of 95.4% were achieved, corresponding to 1 misclassification out of 22 total samples. Cross-validation is an effective way to verify the obtained results, and leave-one-out cross validation (LOOCV) is often used as the validation algorithm [31]. The cross-validation results of oxygenated VOCs are depicted in Fig. 6c, indicating a cross-validation rate of 90.9% was achieved.

Fig. 6d shows a 3D plot of LDA results for all the non-oxygenated VOCs. Points belonged to different VOCs are separated in space, which confirms that the VSA can also discriminate non-oxygenated VOCs. The LDA results of the oxygenated VOCs are depicted in Fig. 6e. Each sample was correctly identified indicating 100% accurate identification of the non-oxygenated VOCs. A correct cross-validation rate of 90.5% was achieved when using the LOOCV, as shown in Fig. 6f.

Finally, to provide a more stringent test of the VSA, the identification ability toward similar VOC mixtures has been investigated. We use the LDA to discriminate the mixtures of EtOH and acetone, EtOH and IPA, acetone and DCM, as well as acetone and MeCN. The concentrations of mixtures during the test are listed in Table S2. Fig. 6g shows a 3D plot of LDA results of the VOCs mixtures. From different view angles, four kinds of VOC mixtures are well separated in a 3D feature space. A correct classification rate of 100% was achieved, as shown in Fig. 6h. The cross-validation results of mixtures are depicted in Fig. 6i, indicating a correct cross-validation rate of 90% has been achieved. These results demonstrate that utilizing the $Ti_3C_2T_x$ based VSA is a promising approach for identification of pure VOCs and similar complex mixtures.

3.6. Concentration prediction of a targeted VOC

The responses of the sensor to ethanol in a background of variable humidity levels and methanol concentrations are shown in Fig. S8. We choose the impedance of the sensor in dry air as the zero point. MXenes also absorb water and methanol [20,21]. Therefore, the MXene-based sensor has drifts when the concentration of ethanol is zero in the presence of water and methanol. When the ethanol concentration is low, the response of the sensor is approximately equal to the linear superposition of the response to water or methanol and the response to ethanol. When the ethanol concentration is relatively high, the response of the sensor is not a linear superposition. This is because the adsorption sites for

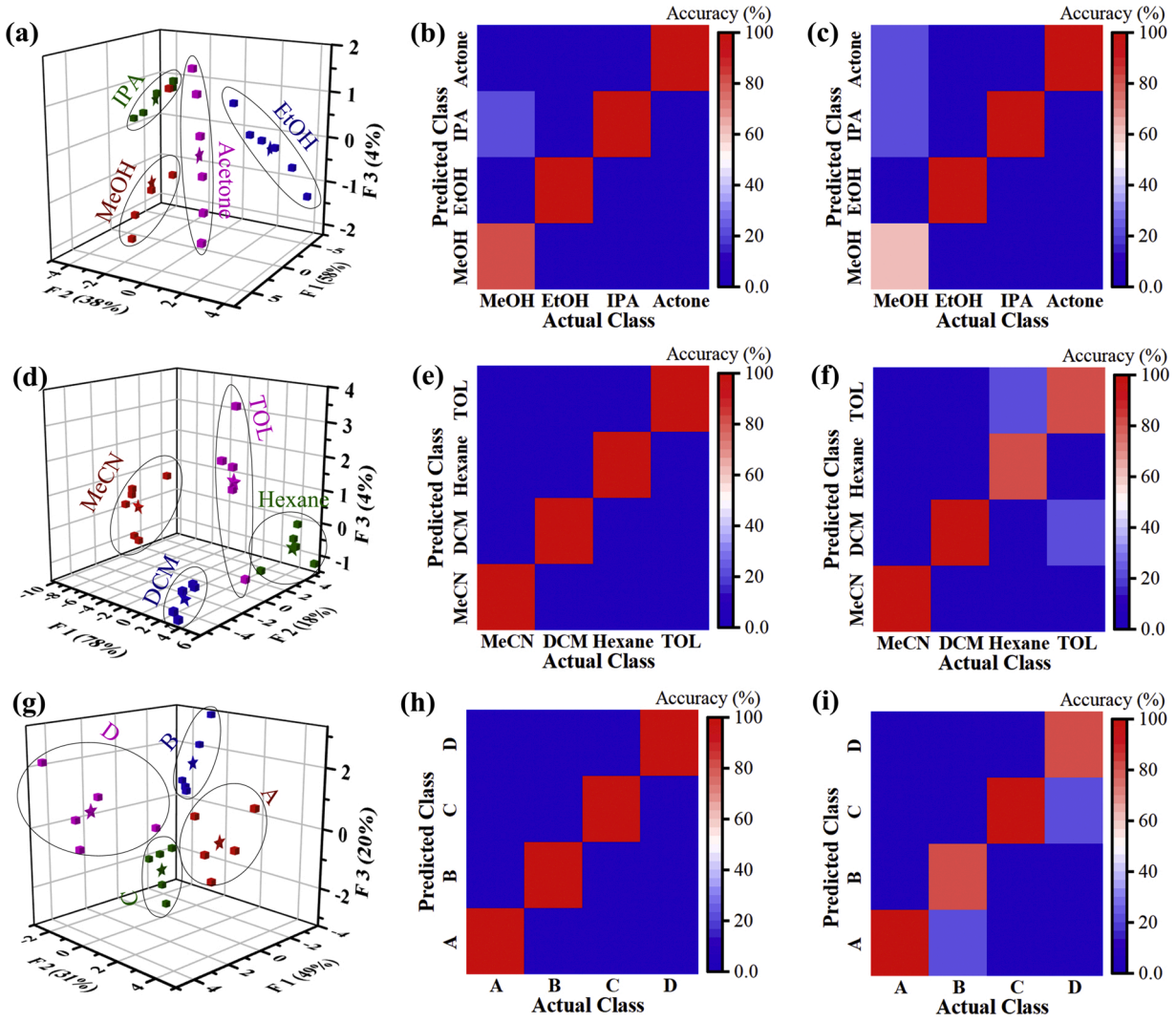

Fig. 6. LDA results of different VOC groups. 3D plot of LDA results the oxygenated VOCs (a), non-oxygenated VOCs (d), and VOC mixtures (g). LDA results of oxygenated VOCs (b), non-oxygenated VOCs (e), and VOC mixtures (h). Cross-validation results of oxygenated VOCs (c), non-oxygenated VOCs (f), and VOC mixtures (i).

ethanol are partially occupied by water or methanol. Therefore, we cannot eliminate the influence of humidity or methanol, just simply detecting a single parameter (e.g., resistance or capacitance).

We used the PLS to quantify concentrations of ethanol in a background of variable humidity levels and methanol concentrations. The number of latent variables (LVs) was selected to provide the minor prediction error without generating an overfitting [44]. Fig. 7a reveals that 5 LVs is the most appropriate LV number for the modeling, based on the root of sum of squared error (SSE) as a function of LV number.

Fig. 7b presents a simple visualization of the quantitative prediction

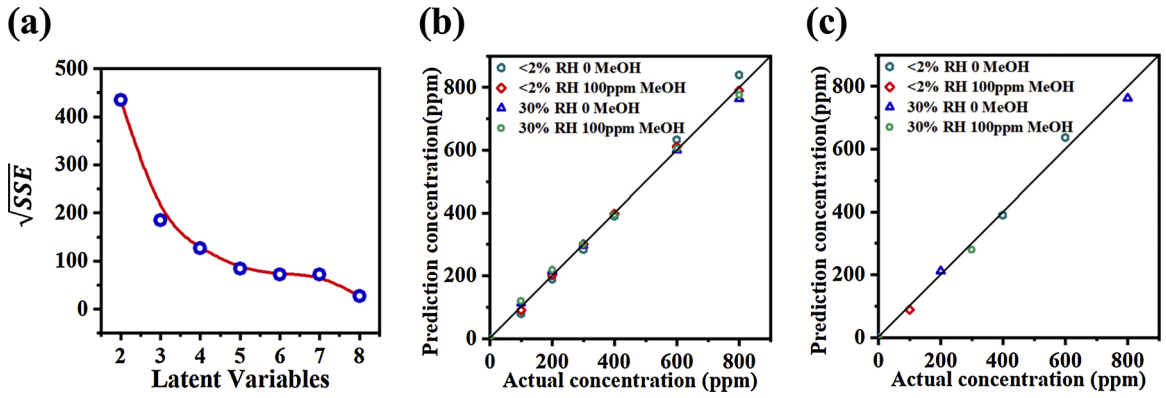

Fig. 7. Ethanol concentration prediction by PLS. (a) The root of SSE varies with the number of LVs. (b) Ethanol concentration prediction in the presence of a variable background. (c) Concentration prediction of second data set.

of ethanol vapors in the presence of variable backgrounds. The position of each point is given by its real concentration (x-axis) and predicted concentration (y-axis). Perfect predictions will lay on the diagonal (i.e., prediction matches the real gas concentration). All the VOC concentrations were predicted quite well, as all the points are close to the diagonal positions. The average accuracy is 93.4% and the root of sum of the squared errors is 83.9 using 5 LVs.

A data set from a second measurement was then used to study the robustness of the determined model. Fig. 7c presents a concentration prediction of second data set using the obtained PLS coefficients from the training set. All the VOC concentrations were predicted quite well, as shown in Fig. 7c, demonstrating that the $Ti_3C_2T_x$ based VSA is an excellent approach for individual VOC concentration prediction in a variable background.

4. Conclusion

In summary, we developed a $Ti_3C_2T_x$ based VSA for selective VOC detection. The VSA was fabricated by depositing a thin film of $Ti_3C_2T_x$ on the surface of an IDE. Eight representative parameters of the proposed VSA were selected as VOC characteristics and the multi-parameters sensing responses create a unique fingerprint for each VOC without temperature change. The VSA showed a high data dimensionality in PCA. Correct rates of 90.9%, 90.5%, and 90% for the identification was achieved for oxygenated VOCs, oxygenated VOCs, and VOCs mixtures in LDA, respectively. The ethanol concentration estimation accuracy is ~93.4% based on the proposed VSA. The high level of identification and concentration prediction shows the potential of MXene based VSAs for detection of VOCs of interest in the presence of known and unknown interferences. We anticipate that the strategy to solve the cross-sensitivity of gas sensors of this work could be easily adapted to other gas sensors and implemented in a range of emerging applications, including agriculture, pollution monitoring, food quality assurance, and medical diagnosis.

CRediT authorship contribution statement

Dongsheng Li: Conceptualization, Data curation, Formal analysis, Writing - original draft. **Guang Liu:** Investigation, Methodology. **Qian Zhang:** Software, Methodology. **Mengjiao Qu:** Validation, Visualization. **Yong Qing Fu:** Writing - review & editing, Supervision. **Qingjun Liu:** Supervision. **Jin Xie:** Project administration, Writing - review & editing, Supervision.

Declaration of Competing Interest

The authors report no declarations of interest.

Acknowledgments

This work is supported in part by the “Zhejiang Provincial Natural Science Foundation of China (LZ19E050002)”, the “National Natural Science Foundation of China (51875521)”, the “Science Fund for Creative Research Groups of National Natural Science Foundation of China (51821093)”.

Appendix A. Supplementary data

Supplementary material related to this article can be found, in the online version, at doi:https://doi.org/10.1016/j.snb.2020.129414.

References

[1] H.M. Fahad, H. Shiraki, M. Amani, C. Zhang, V.S. Hebbar, W. Gao, H. Ota, M. Hettick, D. Kiriya, Y.-Z. Chen, Y.-L. Chueh, A. Javey, Room temperature multiplexed gas sensing using chemical-sensitive 3.5-nm-thin silicon transistors, Sci. Adv. 3 (2017), e1602557.
[2] J. van den Broek, S. Abegg, S.E. Pratsinis, A.T. Guntner, Highly selective detection of methanol over ethanol by a handheld gas sensor, Nat. Commun. 10 (1) (2019) 4220.
[3] S. Cui, H. Pu, S.A. Wells, Z. Wen, S. Mao, J. Chang, M.C. Hersam, J. Chen, Ultrahigh sensitivity and layer-dependent sensing performance of phosphorene-based gas sensors, Nat. Commun. 6 (2015) 8632.
[4] Z. Li, R. Paul, T. Ba Tis, A.C. Saville, J.C. Hansel, T. Yu, J.B. Ristaino, Q. Wei, Non-invasive plant disease diagnostics enabled by smartphone-based fingerprinting of leaf volatiles, Nat. Plants 5 (8) (2019) 856–866.
[5] B. Wang, J.C. Cancilla, J.S. Torrecilla, H. Haick, Artificial sensing intelligence with silicon nanowires for ultraselective detection in the gas phase, Nano Lett. 14 (2) (2014) 933–938.
[6] H. Hu, X. Yang, X. Guo, K. Khaliji, S.R. Biswas, F.J. Garcia de Abajo, T. Low, Z. Sun, Q. Dai, Gas identification with graphene plasmons, Nat. Commun. 10 (1) (2019) 1131.
[7] N. Shehada, G. Bronstrup, K. Funka, S. Christiansen, M. Leja, H. Haick, Ultrasensitive silicon nanowire for real-world gas sensing: noninvasive diagnosis of cancer from breath volatolome, Nano Lett. 15 (2) (2015) 1288–1295.
[8] E. Lee, A. VahidMohammadi, B.C. Prorok, Y.S. Yoon, M. Beidaghi, D.J. Kim, Room temperature gas sensing of two-dimensional titanium carbide (MXene), ACS Appl. Mater. Interfaces 9 (42) (2017) 37184–37190.
[9] X. Liu, T. Ma, N. Pinna, J. Zhang, Two-dimensional nanostructured materials for gas sensing, Adv. Funct. Mater. 27 (2017), 1702168.
[10] W. Yuan, A. Liu, L. Huang, C. Li, G. Shi, High-performance NO2 sensors based on chemically modified graphene, Adv. Mater. 25 (5) (2013) 766–771.
[11] H. Peng, F. Li, Z. Hua, K. Yang, F. Yin, W. Yuan, Highly sensitive and selective room-temperature nitrogen dioxide sensors based on porous graphene, Sens. Actuators B 275 (2018) 78–85.
[12] J.S. Kim, H.W. Yoo, H.O. Choi, H.T. Jung, Tunable volatile organic compounds sensor by using thiolated ligand conjugation on MoS2, Nano Lett. 14 (10) (2014) 5941–5947.
[13] S.-Y. Cho, S.J. Kim, Y. Lee, J.-S. Kim, W.-B. Jung, H.-W. Yoo, J.K.-T. Jung, Highly enhanced gas adsorption properties in vertically aligned MoS2 layers, ACS Nano 9 (9) (2015) 9314–9321.
[14] Q. Li, Y. Cen, J. Huang, X. Li, H. Zhang, Y. Geng, B.I. Yakobson, Y. Du, X. Tian, Zinc oxide-black phosphorus composites for ultrasensitive nitrogen dioxide sensing, Nanoscale Horiz. 3 (5) (2018) 525–531.
[15] E. Lee, A. VahidMohammadi, B.C. Prorok, Y.S. Yoon, M. Beidaghi, D.-J. Kim, Room temperature gas sensing of two-dimensional titanium carbide (MXene), ACS Appl. Mater. Interfaces 9 (42) (2017) 37184–37190.
[16] M. Wu, M. He, Q. Hu, Q. Wu, G. Sun, L. Xie, Z. Zhang, Z. Zhu, A. Zhou, Ti3C2 MXene-based sensors with high selectivity for NH3 detection at room temperature, ACS Sens. 4 (10) (2019) 2763–2770.
[17] M. Naguib, V.N. Mochalin, M.W. Barsoum, Y. Gogotsi, 25th anniversary article: MXenes: a new family of two-dimensional materials, Adv. Mater. 26 (7) (2014) 992–1005.
[18] O. Mashtalir, M. Naguib, B. Dyatkin, Y. Gogotsi, M.W. Barsoum, Kinetics of aluminum extraction from Ti3AlC2 in hydrofluoric acid, Mater. Chem. Phys. 139 (1) (2013) 147–152.
[19] O. Mashtalir, M. Naguib, V.N. Mochalin, Y. Dall'Agnese, M. Heon, M.W. Barsoum, Y. Gogotsi, Intercalation and delamination of layered carbides and carbonitrides, Nat. Commun. 4 (2013) 1716.
[20] S.J. Kim, H.J. Koh, C.E. Ren, O. Kwon, K. Maleski, S.Y. Cho, B. Anasori, C.K. Kim, Y. K. Choi, J. Kim, Y. Gogotsi, H.T. Jung, Metallic Ti3C2Tx MXene gas sensors with ultrahigh signal-to-Noise ratio, ACS Nano 12 (2) (2018) 986–993.
[21] H.J. Koh, S.J. Kim, K. Maleski, S.Y. Cho, Y.J. Kim, C.W. Ahn, Y. Gogotsi, H.T. Jung, Enhanced selectivity of MXene gas sensors through metal ion intercalation: in situ X-ray diffraction study, ACS Sens. 4 (5) (2019) 1365–1372.
[22] S. Sun, M. Wang, X. Chang, Y. Jiang, D. Zhang, D. Wang, Y. Zhang, Y. Lei, W18O49/Ti3C2Tx Mxene nanocomposites for highly sensitive acetone gas sensor with low detection limit, Sens. Actuators B 304 (2020), 127274.
[23] S.H. Lee, W. Eom, H. Shin, R.B. Ambade, J.H. Bang, H.W. Kim, T.H. Han, Room-temperature, highly durable Ti3C2Tx MXene/graphene hybrid fibers for NH3 gas sensing, ACS Appl. Mater. Interfaces 12 (9) (2020) 10434–10442.
[24] E. Lee, A. VahidMohammadi, Y.S. Yoon, M. Beidaghi, D.J. Kim, Two-dimensional vanadium carbide MXene for gas sensors with ultrahigh sensitivity toward nonpolar gases, ACS Sens. 4 (2019) 1603–1611.
[25] A. Lichtenstein, E. Havivi, R. Shacham, E. Hahamy, R. Leibovich, A. Pevzner, V. Krivitsky, G. Davivi, I. Presman, R. Elnathan, Y. Engel, E. Flaxer, F. Patolsky, Supersensitive fingerprinting of explosives by chemically modified nanosensors arrays, Nat. Commun. 5 (2014) 4195.
[26] F. Röck, N. Barsan, U. Weimar, Electronic nose: current status and future trends, Chem. Rev. 108 (2008) 705–725.
[27] N.C. Speller, N. Siraj, B.P. Regmi, H. Marzoughi, C. Neal, I.M. Warner, Rational design of QCM-D virtual sensor arrays based on film thickness, viscoelasticity, and harmonics for vapor discrimination, Anal. Chem. 87 (10) (2015) 5156–5166.
[28] G. Zeng, C. Wu, Y. Chang, C. Zhou, B. Chen, M. Zhang, J. Li, X. Duan, Q. Yang, W. Pang, Detection and discrimination of volatile organic compounds using a single film bulk acoustic wave resonator with temperature modulation as a multiparameter virtual sensor array, ACS Sens. 4 (6) (2019) 1524–1533.
[29] R.A. Potyrailo, R.K. Bonam, J.G. Hartley, T.A. Starkey, P. Vukusic, M. Vasudev, T. Bunning, R.R. Naik, Z. Tang, M.A. Palacios, M. Larsen, L.A. Le Tarte, J. C. Grande, S. Zhong, T. Deng, Towards outperforming conventional sensor arrays with fabricated individual photonic vapour sensors inspired by Morpho butterflies, Nat. Commun. 6 (2015) 7959.

[30] Y. Zhao, Q. Yang, Y. Chang, H. Qu, W. Pang, H. Zhang, X. Duan, Detection and discrimination of volatile organic compounds using a single multi-resonance mode piezotransduced silicon bulk acoustic wave resonator (PSBAR) as virtual sensor array, Sens. Actuators B 254 (2018) 1191–1199.
[31] C. Bur, M. Bastuck, D. Puglisi, A. Schütze, A. Lloyd Spetz, M. Andersson, Discrimination and quantification of volatile organic compounds in the ppb-range with gas sensitive SiC-FETs using multivariate statistics, Sens. Actuators B 214 (2015) 225–233.
[32] H. Liu, Y. He, K. Nagashima, G. Meng, T. Dai, B. Tong, Z. Deng, S. Wang, N. Zhu, T. Yanagida, X. Fang, Discrimination of VOCs molecules via extracting concealed features from a temperature-modulated p-type NiO sensor, Sens. Actuators B 293 (2019) 342–349.
[33] M. Tonezzer, D.T.T. Le, S. Iannotta, N. Van Hieu, Selective discrimination of hazardous gases using one single metal oxide resistive sensor, Sens. Actuators B 277 (2018) 121–128.
[34] M. Tonezzer, Selective gas sensor based on one single SnO2 nanowire, Sens. Actuators B 288 (2019) 53–59.
[35] T. Kuwabara, Y. Kawahara, T. Yamaguchi, K. Takahashi, Characterization of inverted-type organic solar cells with a ZnO layer as the electron collection electrode by ac impedance spectroscopy, ACS Appl. Mater. Interfaces 1 (10) (2009) 2107–2110.
[36] M. Xu, Q. Li, Y. Ma, H. Fan, Ni-doped ZnO nanorods gas sensor: enhanced gas-sensing properties, AC and DC electrical behaviors, Sens. Actuators, B 199 (2014) 403–409.
[37] L. Liu, D. Zhang, Q. Zhang, X. Chen, G. Xu, Y. Lu, Q. Liu, Smartphone-based sensing system using ZnO and graphene modified electrodes for VOCs detection, Biosens. Bioelectron. 93 (2017) 94–101.
[38] X. Li, Y. Chang, Y. Long, Influence of Sn doping on ZnO sensing properties for ethanol and acetone, Mater. Sci. Eng. C 32 (4) (2012) 817–821.
[39] B. Ding, X. Wang, J. Yu, M. Wang, Polyamide 6 composite nano-fiber/net functionalized by polyethyleneimine on quartz crystal microbalance for highly sensitive formaldehyde sensors, J. Mater. Chem. 21 (34) (2011) 12784.
[40] C.E. Ren, K.B. Hatzell, M. Alhabeb, Z. Ling, K.A. Mahmoud, Y. Gogotsi, Charge- and Size-Selective Ion Sieving Through Ti3C2Tx MXene Membranes, J. Phys. Chem. Lett. 6 (20) (2015) 4026–4031.
[41] W.Y. Chen, X. Jiang, S.N. Lai, D. Peroulis, L. Stanciu, Nanohybrids of a MXene and transition metal dichalcogenide for selective detection of volatile organic compounds, Nat. Commun. 11 (1) (2020) 1302.
[42] R.A. Potyrailo, Multivariable sensors for ubiquitous monitoring of gases in the era of internet of things and industrial internet, Chem. Rev. 116 (19) (2016) 11877–11923.
[43] T. Hayasaka, A. Lin, V.C. Copa, L.P. Lopez Jr., R.A. Loberternos, L.I.M. Ballesteros, Y. Kubota, Y. Liu, A.A. Salvador, L. Lin, An electronic nose using a single graphene FET and machine learning for water, methanol, and ethanol, Microsyst. Nanoeng. 6 (2020) 50.
[44] M.G. Nespeca, J.F.V.L. Munhoz, D.L. Flumignan, J.E. de Oliveira, Rapid and sensitive method for detecting adulterants in gasoline using ultra-fast gas chromatography and Partial Least Square Discriminant Analysis, Fuel 215 (2018) 204–211.

Dongsheng Li received the B.E. degree in mechanical engineering from Zhejiang University, Hangzhou, China, in 2018. He is currently pursuing the Ph.D. degree in mechatronic engineering with the School of Mechanical Engineering, Zhejiang University. His current research focuses on the MEMS piezoelectric resonant sensors and actuators and gas sensors.

Jin Xie received the B.Eng. degree from Tsinghua University, Beijing, China, in 2000, the M.Eng. degree from Zhejiang University, Hangzhou, China, in 2003, and the Ph.D. degree from Nanyang Technological University, Singapore, in 2008. From 2007–2011, he worked in Institute of Microelectronics, Singapore. In June 2011, he joined the Department of Mechanical Engineering, University of California, Berkeley, CA, USA, as a post-doc researcher. In October 2012, he joined the School of Mechanical Engineering, Zhejiang University, Hangzhou, China, as a professor. His research interests include micro-electromechanical systems (MEMS) design and processes, micro sensors and actuators.